CFD-Based Frequency Domain Method for Dynamic Stability Derivative Estimation with Application to Transonic Truss-Braced Wing

Nhan Nguyen*
NASA Ames Research Center, Moffett Field, CA 94035
Juntao Xiong†
KBR Wyle, Inc., Moffett Field, CA 94035

This paper presents a dynamic stability estimation technique obtained from high-fidelity CFD simulations of the Mach 0.8 Transonic Truss-Braced Wing (TTBW). A series of unsteady RANS CFD simulations in FUN3D is performed on the TTBW in pitch and plunge oscillations at various reduced frequencies. The time-domain data are transformed into the frequency-domain data by Fourier series. Transfer functions of the dynamic stability derivatives are then estimated by a frequency-domain regression. The dynamic stability derivatives with respect to the angle of attack are determined by the regression of the unsteady aerodynamic coefficients for the plunge motion. The dynamic stability derivatives with respect to the pitch rate are determined by the regression of the differential unsteady aerodynamic coefficients for the pitch motion upon the removal of the angle of attack contribution by the plunge motion. The steady-state stability derivatives are then compared to the results obtained from a stability analysis code VSPAERO as well as steady-state FUN3D simulations. The comparison of the steady-state stability derivatives shows excellent agreement.

I. Introduction

Vehicle stability analysis is an important study to determine both static and dynamic stability of flight vehicles. A set of linearized flight dynamic equations of motion are established to predict the vehicle stability and its motion under applied aerodynamic forces and moments generated by flight control surfaces. Static stability of an aircraft depends on steady state stability derivatives such as C_{m_α} and C_{l_β}. Dynamic stability depends on a larger set of stability derivatives which include both steady state and dynamic stability derivatives. The partial derivatives of the aerodynamic coefficients with respect to the dynamic states of the aircraft are usually called dynamic derivatives such as $C_{L_{\dot\alpha}}$, C_{m_q}, and $C_{m_{\dot q}}$. The dynamic stability derivatives with respect to the angular rates generally can be computed by various analytical techniques. On the other hand, dynamic stability derivatives with respect to the time derivatives of the aircraft states are more difficult to established. These stability derivatives account for the time delay in the aerodynamic response of the aircraft which can be important. The steady state and dynamic stability derivatives can be estimated experimentally by stability-and-control (S&C) wind tunnel experiments or analytically by unsteady flow simulations.

The numerical estimation of dynamic stability derivatives is a current research topic. Recent work in this area can be found in many references.[1–3] Many of these technique do not adequately capture the various terms of the dynamic stability derivatives. More importantly, the effects of the frequency response on the dynamic stability derivatives is not well addressed. Murman uses reduced-frequency approach to address the frequency response, but the approach lacks sufficient details to enable a systematic approach to determining the dynamic stability derivatives.

This paper presents a method for estimating the dynamic stability derivatives in the frequency domain. The approach addresses sufficiently the effects of the frequency response on the dynamic stability derivatives. Using unsteady RANS CFD simulation results, the time histories of the aerodynamic coefficients are converted in the frequency domain as a function of the reduced frequency. A frequency-domain transfer function is designed to capture both the

*Senior Research Scientist and Technical Group Lead of Advanced Control and Engineering Systems Group, Intelligent Systems Division, nhan.t.nguyen@nasa.gov
†Aerospace Engineer, Intelligent System Division, juntao.xiong@nasa.gov

steady state and dynamic derivatives. The transfer function is formulated based on the Theodorsen's theory.[4] A frequency-domain regression analysis is then performed to estimate the transfer function. The proposed method can estimate those dynamic stability derivatives that are usually not captured in many analyses but do exist in the Theordorsen's theory such as $C_{m_{\ddot{q}}}$ due to the apparent mass effect.

The proposed method is applied to the Transonic Truss-Braced Wing (TTBW). The Subsonic Ultra Green Aircraft Research (SUGAR) Transonic Truss-Braced Wing aircraft concept is a Boeing-developed N+3 aircraft configuration funded by the NASA ARMD Advanced Air Transport Technologies (AATT) project.[5,6] The TTBW aircraft concept is designed to be aerodynamically efficient by employing a wing aspect ratio of about 19.55 which is significantly greater than those of cantilever wing transport configurations. For example, the latest Boeing 777-X is reported to have a wing aspect ratio of 11. Without structural bracing, the increase in the wing root bending moment would require a significant structural reinforcement which would lead to an increase in the structural weight that would offset the aerodynamic benefit of the high aspect ratio wing. Thus, the design of a truss-braced structure is a multidisciplinary design optimization process that strives to achieve a delicate balance between aerodynamic efficiency and structural efficiency. In the SUGAR configuration, the trade between the aerodynamic performance and structural design results in a truss-braced configuration with the wings braced at approximately mid-span by two main struts. In addition, two jury struts, one on each wing, provide the additional structural reinforcement. Two versions of the TTBW configurations are currently being developed by Boeing; a Mach 0.745 version and a Mach 0.8 version. Figure 1 is an illustration of the Mach 0.8 TTBW aircraft.

Figure 1. Boeing Mach 0.8 Transonic Truss-Braced Wing Aircraft Concept

A series of 3D unsteady RANS simulations using the CFD code FUN3D is performed for both the Mach 0.745 and Mach 0.8 TTBW in pitch, plunge, roll, and yaw oscillations. For each simulation, the motion of the TTBW described by the pitch angle θ, altitude h, roll or bank angle ϕ, and yaw or heading angle ψ is subjected to a pure sinusoidal input at a specified frequency, expressed in terms of the reduced frequency parameter $k = \dfrac{\omega \bar{c}}{2V_\infty}$ for the pitch and plunge oscillations and $k = \dfrac{\omega b}{2V_\infty}$ for the roll and yaw oscillations. The reduced frequency varies from 0.02 to 0.2 in the simulations. The results are computed by the proposed method and then compared to the results obtained from a stability analysis code, VSPAERO.

II. Stability Derivative Estimation Method

Consider a pitch oscillation of an aircraft where the pitch angle θ varies sinusoidally at a given frequency ω

$$\theta = \bar{\theta} + \tilde{\theta} \tag{1}$$

$$\tilde{\theta} = \theta_0 \sin \omega t = \theta_0 \sin k\tau \tag{2}$$

where $\bar{\theta}$ is the mean pitch angle, $\tilde{\theta}$ is the oscillating pitch angle, $\tau = \frac{2V_\infty t}{c}$ is a non-dimensional time, V_∞ is the freestream airspeed, c is the airfoil chord, and k is the reduced frequency. The flight path angle γ is defined as

$$\gamma = \theta - \alpha \tag{3}$$

If the flight path angle γ is zero, then the pitch angle θ is equal to the angle of attack α. The pitch rate q is the time derivative of the pitch angle, i.e., $q = \dot{\theta}$ if the bank angle ϕ and heading angle ψ are zero. It should be noted that some references in the literature make the equivalency between $\dot{\theta}$ and $\dot{\alpha}$, but generally these time derivatives are not the same.

The effects of the angle of attack and pitch angle are not always equivalent. The angle of attack α is defined as

$$\alpha = \tan^{-1} \frac{w}{u} \tag{4}$$

where w is the vertical airspeed component and u is the axial airspeed component. For small angles of attack, $u \approx V_\infty$ and $w \approx \alpha V_\infty$. The vertical airspeed w, which is constant along the aircraft fuselage, can be determined by the change in the altitude. A change in the altitude creates a vertical airspeed which changes the angle of attack. When an aircraft is pitched about its center of gravity (CG), the pitch rate q creates a linearly varying vertical airspeed along the aircraft fuselage. This induced vertical airspeed causes changes in the aerodynamic lift and pitching moment in a different way than the changes in the vertical airspeed created by changes in the altitude. The horizontal tail plays a dominant role in the dynamic stability derivatives with respect to the pitch rate, whereas the wing contributes largely to the stability derivatives with respect to the angle of attack.

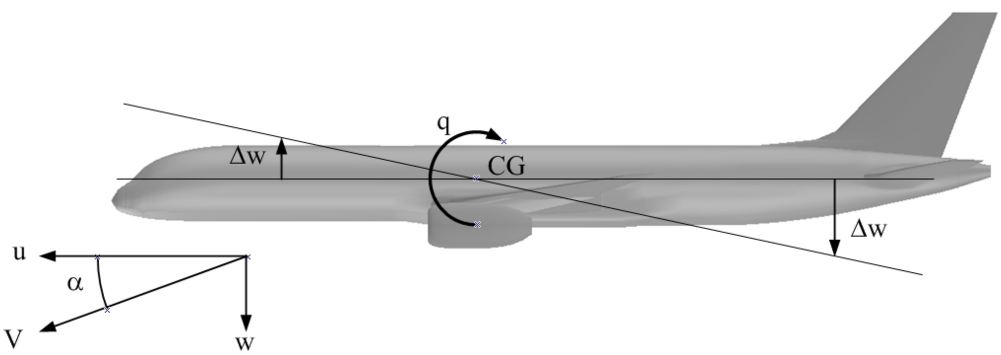

Figure 2. Effect of Pitch Rate on Aerodynamics

A. Frequency-Domain Formulation

The dynamic stability of an aircraft can be explained by the Theodorsen's theory which presents an analytical method for determining the lift and pitching moment of an airfoil in pitch oscillations in incompressible flow. The unsteady lift coefficient $\tilde{c}_l$ is established by the Theodorsen's theory as

$$\tilde{c}_l = c_{l_c} + c_{l_{nc}} \tag{5}$$

where c_{l_c} is the so-called circulatory lift coefficient and $c_{l_{nc}}$ is the so-called noncirculatory lift coefficient. The circulatory lift coefficient c_{l_c} is given by

$$c_{l_c} = c_{l_\alpha} C(k) \left(\tilde{\theta} + e_c \frac{\dot{\theta}}{V_\infty} \right) = c_{l_\alpha} C(k) \left(\tilde{\theta} + 2 \frac{e_c}{c} \frac{d\theta}{d\tau} \right) = c_{l_\alpha} C(k) \left(\tilde{\theta} + 2 \frac{e_c}{c} \frac{cq}{2V_\infty} \right) \tag{6}$$

where $\frac{d\theta}{d\tau} = \frac{cq}{2V_\infty}$ is the nondimensional pitch rate, c_{l_α} is the lift curve slope which is equal to 2π for incompressible flow, c is the chord length, and e_c is the distance from the pitch center to the three-quarter chord point which is positive when the pitch center lies forward of the three-quarter chord point. The complex-valued Theodorsen's function $C(k)$ is usually expressed as

$$C(k) = F(k) + iG(k) \tag{7}$$

The noncirculatory lift coefficient $c_{l_{nc}}$ is due to the inertial force acting on the oscillating airfoil and is given by

$$c_{l_{nc}} = c_{l_\alpha}\left(\frac{c\dot{\theta}}{4V_\infty} + \frac{e_m c\ddot{\theta}}{4V_\infty^2}\right) = c_{l_\alpha}\left(\frac{1}{2}\frac{d\theta}{d\tau} + \frac{e_m}{c}\frac{d^2\theta}{d\tau^2}\right) = c_{l_\alpha}\left(\frac{1}{2}\frac{cq}{2V_\infty} + \frac{e_m}{c}\frac{c^2\dot{q}}{4V_\infty^2}\right) \tag{8}$$

where $\frac{d\theta}{d\tau} = \frac{c^2\dot{q}}{4V_\infty^2}$ is the nondimensional pitch acceleration due to the apparent mass effect and e_m is the distance from the pitch center to the mid-chord point, which is positive when the pitch center lies forward of the mid-chord point.

For zero flight path angle, $\tilde{\theta} = \tilde{\alpha}$. Thus, the unsteady lift coefficient $\tilde{c}_l$ can be expressed as

$$\tilde{c}_l = c_{l_\alpha}\left[C(k)\left(\tilde{\alpha} + 2\frac{e_c}{c}\frac{cq}{2V_\infty}\right) + \frac{1}{2}\frac{cq}{2V_\infty} + \frac{e_m}{c}\frac{c^2\dot{q}}{4V_\infty^2}\right] \tag{9}$$

The unsteady pitching moment coefficient $\tilde{c}_m$ is treated by Theodorsen's theory in a similar manner where it is comprised of the circulatory and noncirculatory components and is given by

$$\tilde{c}_m = c_{l_\alpha}\left[C(k)\frac{e}{c}\left(\tilde{\alpha} + 2\frac{e_c}{c}\frac{cq}{2V_\infty}\right) - \frac{1}{2}\frac{e_c}{c}\frac{cq}{2V_\infty} - \left(\frac{1}{32} + \frac{e_m^2}{c^2}\right)\frac{c^2\dot{q}}{4V_\infty^2}\right] \tag{10}$$

where e is the distance from the pitch center to the quarter-chord point which is positive when the pitch center lies aft of the quarter-chord point. The unsteady lift and pitching moment coefficient are therefore functions of the angle of attack, pitch rate, and pitch acceleration.

The motion of an airfoil in plunge is related to the pitching motion by the angle of attack

$$\tilde{\alpha} = \frac{\dot{h}}{V_\infty} \tag{11}$$

where $\dot{h} = w$ is the vertical airspeed which is positive in the downward direction as shown in Fig. 2.

The unsteady lift coefficient for an airfoil in plunge according to the Theodorsen's theory is expressed as

$$\tilde{c}_l = c_{l_\alpha}\left[C(k)\frac{\dot{h}}{V_\infty} + \frac{c\ddot{h}}{4V_\infty^2}\right] = c_{l_\alpha}\left[C(k)\tilde{\alpha} + \frac{1}{2}\frac{d\alpha}{d\tau}\right] = c_{l_\alpha}\left[C(k)\tilde{\alpha} + \frac{1}{2}\frac{c\dot{\alpha}}{2V_\infty}\right] \tag{12}$$

where $\frac{d\alpha}{d\tau} = \frac{c\dot{\alpha}}{2V_\infty}$ is the nondimensional angle of attack rate due to the apparent mass effect.

The pitching moment coefficient for an airfoil in plunge is given by

$$\tilde{c}_m = c_{l_\alpha}\left[C(k)\frac{e}{c}\tilde{\alpha} - \frac{1}{2}\frac{e_m}{c}\frac{d\alpha}{d\tau}\right] = c_{l_\alpha}\left[C(k)\frac{e}{c}\tilde{\alpha} - \frac{1}{2}\frac{e_m}{c}\frac{c\dot{\alpha}}{2V_\infty}\right] \tag{13}$$

To isolate the effect of pitch dynamics in the unsteady lift and pitching moment coefficient, the angle of attack contribution must be removed from Eqs. (9) and (10). This can be accomplished by subtracting the unsteady lift and pitching moment for the plunge motion from those for the pitch motion. These differential unsteady lift and pitching moment coefficients are expressed as

$$\Delta\tilde{c}_l = c_{l_\alpha}\left[C(k)2\frac{e_c}{c}\frac{cq}{2V_\infty} + c_{l_\alpha}\left(\frac{1}{2}\frac{cq}{2V_\infty} + \frac{e_m}{c}\frac{c^2\dot{q}}{4V_\infty}\right) - \frac{1}{2}\frac{c\dot{\alpha}}{2V_\infty}\right] \tag{14}$$

$$\Delta\tilde{c}_m = c_{l_\alpha}\left[C(k)2\frac{e}{c}\frac{e_c}{c}\frac{cq}{2V_\infty} - \frac{1}{2}\frac{e_c}{c}\frac{cq}{2V_\infty} - \left(\frac{1}{32} + \frac{e_m^2}{c^2}\right)\frac{c^2\dot{q}}{4V_\infty} + \frac{1}{2}\frac{e_m}{c}\frac{c\dot{\alpha}}{2V_\infty}\right] \tag{15}$$

The acceleration rate terms in the differential unsteady lift and pitching moment coefficients are usually quite small and can be neglected. Alternatively, they can be accounted for quite easily if they can be estimated from the dynamic stability derivative estimation.

Using the Theodorsen's theory as a guide, we formulate the following form of the unsteady lift coefficient for an aircraft in pure pitch oscillations as

$$\tilde{C}_L = C_{L_{\tilde{\alpha}}}(k)\left(\tilde{\alpha} + a_1 \frac{d\theta}{d\tau}\right) + a_2 \frac{d\theta}{d\tau} + a_3 \frac{d^2\theta}{d\tau^2} \tag{16}$$

where $C_{L_{\tilde{\alpha}}}(k)$ is a frequency-domain transfer function analogous to the Theordorsen's function with zero imaginary part at $k = 0$. We also formulate the following form of the unsteady lift coefficient for an aircraft in pure plunge oscillations as

$$\tilde{C}_L = C_{L_{\tilde{\alpha}}}(k)\,\tilde{\alpha} + b_1 \frac{d\alpha}{d\tau} \tag{17}$$

For a general motion of an aircraft, we express the unsteady lift coefficient as

$$\tilde{C}_L = C_{L_{\tilde{\alpha}}}(k)\,\tilde{\alpha} + b_1 \frac{d\alpha}{d\tau} + C_{L_{\tilde{\alpha}}}(k)\,a_1 \frac{d\theta}{d\tau} + a_2 \frac{d\theta}{d\tau} + a_3 \frac{d^2\theta}{d\tau^2} \tag{18}$$

where the reduced frequency is based on the mean aerodynamic chord $\bar{c}$.

In the dimensional form, the unsteady lift coefficient is expressed as

$$C_L = C_{L_0} + C_{L_\alpha}\bar{\alpha} + C_{L_{\tilde{\alpha}}}(k)\,\tilde{\alpha} + C_{L_{\dot{\alpha}}} \frac{\bar{c}\dot{\alpha}}{2V_\infty} + C_{L_{\tilde{q}}}(k)\,\frac{\bar{c}q}{2V_\infty} + C_{L_{\dot{q}}} \frac{\bar{c}^2\dot{q}}{4V_\infty^2} \tag{19}$$

We note that the unsteady lift curve slope $C_{L_{\tilde{\alpha}}}(k)$ is a function of the reduced frequency and is equal to C_{L_α} only when $k = 0$. Thus, $C_{L_{\tilde{\alpha}}}(k)$ is a dynamic stability derivative whereas C_{L_α} is the steady state derivative when $k = 0$. Similarly, the dynamic stability derivative $C_{L_{\tilde{q}}}(k)$ gives C_{L_q} when $k = 0$, but C_{L_q} is considered a dynamic stability since the pitch rate is a dynamic state variable of an aircraft.

The unsteady pitching moment coefficient can be formulated the same way as

$$C_m = C_{m_0} + C_{m_\alpha}\bar{\alpha} + C_{m_{\tilde{\alpha}}}(k)\,\tilde{\alpha} + C_{m_{\dot{\alpha}}} \frac{\bar{c}\dot{\alpha}}{2V_\infty} + C_{m_{\tilde{q}}}(k)\,\frac{\bar{c}q}{2V_\infty} + C_{m_{\dot{q}}} \frac{\bar{c}^2\dot{q}}{4V_\infty^2} \tag{20}$$

In preliminary aircraft stability analyses, the frequency dependency of the stability derivatives is usually ignored. While the dynamic stability derivatives $C_{L_{\dot{\alpha}}}$ and $C_{\dot{\alpha}}$ can be estimated by the Theodorsen's theory, the dynamic stability derivatives $C_{L_{\dot{q}}}$ and $C_{m_{\dot{q}}}$ are also usually ignored.

In the current study, we will use the CFD simulation data for the plunge motion for the dynamic stability derivative estimation due to the angle of attack dynamics and the difference in the CFD simulation data between the pitch and plunge motions for the dynamic stability derivative estimation due to the pitch rate dynamics. That is, the differential unsteady lift and pitching moment coefficients for use in the dynamic stability derivative estimation due to the pitch rate dynamics are of the form

$$\Delta\tilde{C}_L = \left[C_{L_{\tilde{\alpha}}}(k)\,a_1 + a_2\right] \frac{d\theta}{d\tau} + a_3 \frac{d^2\theta}{d\tau^2} \tag{21}$$

$$\Delta\tilde{C}_m = \left[C_{m_{\tilde{\alpha}}}(k)\,c_1 + c_2\right] \frac{d\theta}{d\tau} + c_3 \frac{d^2\theta}{d\tau^2} \tag{22}$$

These quantities are computed in the following section.

B. Frequency-Domain Regression

The response of the unsteady lift coefficient of an aircraft to a sinusoidal plunge motion described by Eq. (2) is

$$\tilde{C}_L = (U + iW)\,\tilde{\theta} = (U + iW)\,\theta_0 \sin k\tau \tag{23}$$

This is valid so long as the amplitude of the plunge motion is sufficiently small so that nonlinear aerodynamic effects become significant. The quantities U and W are the real part and imaginary part of the dynamic stability derivatives $C_{L_{\tilde{\alpha}}}(k)$ which can be computed from the Fourier series as

$$U(k) = \frac{k\int_0^{\frac{2n\pi}{k}} \tilde{C}_L \sin k\tau d\tau}{n\pi\theta_0} \tag{24}$$

$$W(k) = \frac{k\int_0^{\frac{2n\pi}{k}} \tilde{C}_L \cos k\tau d\tau}{n\pi\theta_0} \tag{25}$$

We express

$$\tilde{C}_L = C_{L_{\tilde{\alpha}}}(k)\,\tilde{\alpha} + b_1\frac{d\alpha}{d\tau} \tag{26}$$

Let $\bar{s} = ik$ be the nondimensional Laplace variable, then we express

$$\tilde{C}_L = \left[H(\bar{s})\,c_0 + c_1\bar{s}\right]\tilde{\alpha} \tag{27}$$

where $H(\bar{s})$ is a unit magnitude transfer function such that

$$H(\bar{s})\,c_0 = C_{L_{\tilde{\alpha}}}(k) \tag{28}$$

Taking the partial derivative of $\tilde{C}_L$ with respect to $\tilde{\alpha}$, we obtain the transfer function from the angle of attack to the unsteady lift coefficient in the frequency domain

$$\frac{\partial C_L}{\partial\tilde{\alpha}}(\bar{s}) = H(\bar{s})\,c_0 + c_1\bar{s} \tag{29}$$

The unsteady pitching moment coefficient is analyzed in the same way as the lift coefficient and is expressed as

$$\frac{\partial C_m}{\partial\tilde{\alpha}}(\bar{s}) = G(\bar{s})\,d_0 + d_1\bar{s} \tag{30}$$

The transfer function $H(\bar{s})$ must have zero imaginary part at $\bar{s} = 0$ and also must be a stable and proper transfer function. From linear systems theory, a proper transfer function is expressed as a rational fraction with the polynomial in the numerator having a degree no greater than the degree of the polynomial in the denominator. A stable transfer function has stable poles which are the roots of the polynomial in the denominator. All stable poles must have negative real part.

The selection of the transfer function $H(\bar{s})$ is essential in the estimation of the dynamic stability derivatives. A good selection of $H(\bar{s})$ ensures a goodness of fit of the frequency response data in the frequency domain. The selection of the stable poles are also important. To ensure exponential decay in the response, the stable poles should not be complex as this will result in an amplification at the resonant frequency which is determined by the imaginary part of the poles. A general expression of the transfer function $H(\bar{s})$ is given by

$$H(\bar{s}) = 1 + \frac{\sum_{i=1}^{m} a_i\bar{s}^i}{\bar{s}^n + \sum_{i=0}^{n-1} b_i\bar{s}^i} \tag{31}$$

where $m \leq n$. The denominator polynomial is also expressed as

$$\bar{s}^n + \sum_{i=0}^{n-1} b_i\bar{s}^i = \Pi_{i=1}^{n}(\bar{s} - p_i) \tag{32}$$

where p_i is a pole such that $p_i < 0$ for all $i = 1, \ldots, n$.

The simplest transfer function is a second-order transfer function

$$H(\bar{s}) = 1 + \frac{a_2\bar{s}^2 + a_1\bar{s}}{\bar{s}^2 + b_1\bar{s} + b_0} \tag{33}$$

In some instances, a higher-order transfer function may be necessary to provide a better regression of the frequency-domain data for complex flow in transonic regime. Transonic correction methods based on the Theodorsen's theory has been developed.[7–10] A frequency-domain regression is performed to compute the coefficients of the unsteady lift coefficient. Assuming $m = n$ is even, then the transfer function $\frac{\partial C_L}{\partial \tilde{\alpha}}(\bar{s})$ can be expressed as

$$\frac{\partial C_L}{\partial \tilde{\alpha}}(\bar{s}) = \frac{\sum_{j=0}^{n+1} e_j (ik)^j}{(ik)^n + \sum_{l=0}^{n-1} b_l (ik)^l} = \frac{\sum_{j=0\text{ even}}^{n} (-1)^{\frac{j}{2}} e_j k^j + i \sum_{l=1\text{ odd}}^{n+1} (-1)^{\frac{l-1}{2}} e_l k^l}{(-1)^{\frac{n}{2}} k^n + \sum_{j=0\text{ even}}^{n-2} (-1)^{\frac{j}{2}} b_j k^j + i \sum_{l=1\text{ odd}}^{n-1} (-1)^{\frac{l-1}{2}} b_l k^l} \tag{34}$$

The estimation error between the transfer function and the frequency domain data is expressed as

$$\begin{aligned}
\varepsilon =& \frac{\partial C_L}{\partial \tilde{\alpha}}(\bar{s}) - [U(k) + iW(k)] \\
=& \frac{\sum_{j=0}^{n+1} e_j (ik)^j}{(ik)^n + \sum_{l=0}^{n-1} b_l (ik)^l} - [U(k) + iW(k)] \\
=& \frac{\sum_{j=0\text{ even}}^{n} (-1)^{\frac{j}{2}} e_j k^j - U(k)\left[(-1)^{\frac{n}{2}} k^n + \sum_{j=0\text{ even}}^{n-2} (-1)^{\frac{j}{2}} b_j k^j\right] + W(k) \sum_{l=1\text{ odd}}^{n-1} (-1)^{\frac{l-1}{2}} b_l k^l}{(-1)^{\frac{n}{2}} k^n + \sum_{j=0\text{ even}}^{n-2} (-1)^{\frac{j}{2}} b_j k^j + i \sum_{l=1\text{ odd}}^{n-1} (-1)^{\frac{l-1}{2}} b_l k^l} \\
&+ \frac{i\left\{\sum_{l=1\text{ odd}}^{n+1} (-1)^{\frac{l-1}{2}} e_l k^l - U(k) \sum_{l=1\text{ odd}}^{n-1} (-1)^{\frac{l-1}{2}} b_l k^l - W(k)\left[(-1)^{\frac{n}{2}} k^n + \sum_{j=0\text{ even}}^{n-2} (-1)^{\frac{j}{2}} b_j k^j\right]\right\}}{(-1)^{\frac{n}{2}} k^n + \sum_{j=0\text{ even}}^{n-2} (-1)^{\frac{j}{2}} b_j k^j + i \sum_{l=1\text{ odd}}^{n-1} (-1)^{\frac{l-1}{2}} b_l k^l}
\end{aligned} \tag{35}$$

The estimation error goes to zero if the magnitude of the numerator is zero. Thus, the estimation of the transfer function can be obtained by minimizing the magnitude square of the numerator of the estimation error by the following cost function:

$$\begin{aligned}
J =& \frac{1}{2} \sum_{N=1}^{M} \left\{ \sum_{j=0\text{ even}}^{n} (-1)^{\frac{j}{2}} e_j k_N^j - U(k_N)\left[(-1)^{\frac{n}{2}} k_N^4 + \sum_{j=0\text{ even}}^{n-2} (-1)^{\frac{j}{2}} b_j k_N^j\right] + W(k_N) \sum_{l=1\text{ odd}}^{n-1} (-1)^{\frac{l-1}{2}} b_l k_N^l \right\}^2 \\
&+ \frac{1}{2} \sum_{N=1}^{M} \left\{ \sum_{l=1\text{ odd}}^{n+1} (-1)^{\frac{l-1}{2}} e_l k_N^l - U(k_N) \sum_{l=1\text{ odd}}^{n-1} (-1)^{\frac{l-1}{2}} b_l k_N^l - W(k_N)\left[(-1)^{\frac{n}{2}} k_N^4 + \sum_{j=0\text{ even}}^{n-2} (-1)^{\frac{j}{2}} b_j k_N^j\right] \right\}^2
\end{aligned} \tag{36}$$

The estimation is performed over a data set of M data points. The standard method for minimization is to take the partial derivatives of J with respect to the coefficients e_i and b_i and then set them to zero. This yields

$$\begin{aligned}
\frac{\partial J}{\partial e_m} =& \sum_{N=1}^{M} \sum_{j=0\text{ even}}^{n} (-1)^{\frac{m+j}{2}} e_j k_N^{m+j} - \sum_{N=1}^{M} U(k_N) (-1)^{\frac{m+n}{2}} k_N^{m+n} - \sum_{N=1}^{M} U(k_N) \sum_{j=0\text{ even}}^{n-2} (-1)^{\frac{m+j}{2}} b_j k_N^{m+j} \\
&+ \sum_{N=1}^{M} W(k_N) \sum_{l=1\text{ odd}}^{n-1} (-1)^{\frac{m+l-1}{2}} b_l k_N^{m+l} = 0,\ m = 0, \ldots, n+2 \text{ even}
\end{aligned} \tag{37}$$

$$\begin{aligned}
\frac{\partial J}{\partial e_r} =& \sum_{N=1}^{M} \sum_{l=1\text{ odd}}^{n+1} (-1)^{\frac{r+l-2}{2}} e_l k_N^{r+l} - \sum_{N=1}^{M} U(k_N) \sum_{l=1\text{ odd}}^{n-1} (-1)^{\frac{r+l-2}{2}} b_l k_N^{r+l} - \sum_{N=1}^{M} W(k_N) (-1)^{\frac{r+n-1}{2}} k_N^{r+n} \\
&- \sum_{N=1}^{M} W(k_N) \sum_{j=0\text{ even}}^{n-2} (-1)^{\frac{r+j-1}{2}} b_j k_N^{r+j} = 0,\ \ r = 1, \ldots, n+1 \text{ odd}
\end{aligned} \tag{38}$$

$$\begin{aligned}
\frac{\partial J}{\partial b_m} =& -\sum_{N=1}^{M} U(k_N) \sum_{j=0\text{ even}}^{n} (-1)^{\frac{m+j}{2}} e_j k_N^{m+j} - \sum_{N=1}^{M} W(k_N) \sum_{l=1\text{ odd}}^{n+1} (-1)^{\frac{m+l-1}{2}} e_l k_N^{m+l} \\
&+ \sum_{N=1}^{M} \left[U^2(k_N) + W^2(k_N)\right] (-1)^{\frac{m+n}{2}} k_N^{m+n} \\
&+ \sum_{N=1}^{M} \left[U^2(k_N) + W^2(k_N)\right] \sum_{j=0\text{ even}}^{2} (-1)^{\frac{m+j}{2}} b_j k_N^{m+j} = 0,\ m = 0, \ldots, n \text{ even}
\end{aligned} \tag{39}$$

$$\frac{\partial J}{\partial b_r} = \sum_{N=1}^{M} W(k_N) \sum_{j=0 \text{ even}}^{n} (-1)^{\frac{r+j-1}{2}} e_j k_N^{r+j} - \sum_{N=1}^{M} U(k_N) \sum_{l=1 \text{ odd}}^{n+1} (-1)^{\frac{r+l-2}{2}} e_l k_N^{r+l}$$

$$+ \sum_{N=1}^{M} \left[U^2(k_N) + W^2(k_N)\right] \sum_{l=1 \text{ odd}}^{n-1} (-1)^{\frac{r+l-2}{2}} b_l k_N^{r+l} = 0,\ r = 1,\ldots,n-1 \text{ odd} \tag{40}$$

The resulting equations can be cast in a matrix equation of the form

$$Ax = B \tag{41}$$

which can be solved for the coefficients e_i and b_i.

However, by estimating the coefficients b_i, the possibility of unstable or complex poles may exist if there are not enough data over a sufficiently large frequency range. Therefore, a strategy is to constrain the poles to be negative real. The poles typically would satisfy the condition $\left|\max_{i=1}^{n} p_i\right| \leq \max_{N=1}^{M} k_N$ for low-order transfer functions. This is to ensure that the poles are not unrealistically set too far outside the frequency bandwidth of the data. The poles can be optimized by an exhaustive search method with the values generated by a random function. In so doing, the minimization becomes a constrained optimization problem posed by the following cost function

$$J = \frac{1}{2} |\varepsilon|^2 \tag{42}$$

subject to the constraints specified by Eqs. (37) and (38).

Once the coefficients e_i and b_i are determined, the coefficients a_i and c_i are determined next by solving a set of nonlinear equations that map the coefficients e_i and b_i to the coefficients a_i and c_i. Consider the second-order transfer function $\frac{\partial C_L}{\partial \tilde{\alpha}}(\bar{s})$, the coefficients a_i and c_i are determined from

$$\frac{e_3\bar{s}^3 + e_2\bar{s}^2 + e_1\bar{s} + e_0}{\bar{s}^2 + b_1\bar{s} + b_0} = \left(1 + \frac{a_2\bar{s}^2 + a_1\bar{s}}{\bar{s}^2 + b_1\bar{s} + b_0}\right) c_0 + c_1 \tag{43}$$

The use of the nondimensional Laplace variable allows the frequency domain expression of the unsteady aerodynamic coefficients to be readily converted into the time domain. Consider the second-order transfer function $H(\bar{s})$ which can be expressed in a partial fraction form as

$$H(\bar{s}) = 1 + \frac{a_2\bar{s}^2 + a_1\bar{s}}{\bar{s}^2 + b_1\bar{s} + b_0} = 1 + a_2 + \frac{r_1}{\bar{s} - p_1} + \frac{r_2}{\bar{s} - p_2} \tag{44}$$

where p_1 and p_2 are the poles which are the roots of the denominator polynomial, and r_1 and r_2 are the residues which can be determined. We then express the unsteady lift coefficient in the time domain as

$$\tilde{C}_L = (1 + a_2) c_0 \alpha + c_1 \frac{\bar{c}\dot{\alpha}}{2V_\infty} + c_0 (\mu_1 + \mu_2) \tag{45}$$

where μ_1 and μ_2 are functions of the angle of attack α determined from the following differential equations:

$$\frac{\bar{c}\dot{\mu}_1}{2V_\infty} = p_1 \mu_1 + r_1 \alpha \tag{46}$$

$$\frac{\bar{c}\dot{\mu}_2}{2V_\infty} = p_2 \mu_2 + r_2 \alpha \tag{47}$$

The dynamic stability derivative estimation for the pitch rate dynamics can be performed in the same manner using the differential unsteady lift and pitching moment coefficients with can be computed as follows. The differential unsteady lift coefficient is computed as

$$\Delta\tilde{C}_L = (T + iV)\tilde{\alpha} - C_{L_{\tilde{\alpha}}}\tilde{\alpha} \tag{48}$$

where $T(k)$ and $V(k)$ are the Fourier sine and cosine series coefficients obtained from the unsteady lift coefficient for the pitch motion, and $C_{L_{\tilde{\alpha}}}(k)$ is the dynamic stability derivative obtained from the plunge motion as computed by Eq.

(28). By subtracting off the angle of attack contribution from the unsteady lift coefficient, the differential unsteady lift coefficient $\Delta\tilde{C}_L$ is a function of the pitch rate only and therefore can be expressed as

$$\Delta\tilde{C}_L = (Q + iP)\frac{d\theta}{d\tau} \tag{49}$$

Equating Eq. (48) to Eq. (49), we obtain

$$Q = \frac{V - \Im(H(s))c_0}{k} \tag{50}$$

$$P = \frac{-T + \Re(H(s))c_0}{k} \tag{51}$$

Alternatively, the differential unsteady lift coefficient can be computed by subtracting the unsteady lift coefficient for the plunge motion from that for the pitch motion. This is expressed as

$$\Delta\tilde{C}_L = (T + iV)\tilde{\alpha} - (U + iW)\tilde{\alpha} + C_{L_{\dot{\alpha}}}\bar{s}\tilde{\alpha} \tag{52}$$

where $C_{L_{\dot{\alpha}}}$, which is constant, is the dynamic stability derivative with respect to the angle of attack rate obtained from the plunge motion. Hence, we have

$$Q = \frac{V - W + kC_{L_{\dot{\alpha}}}}{k} \tag{53}$$

$$P = \frac{-T + U}{k} \tag{54}$$

C. Dynamic Stability Derivatives Due to Unsteady Drag Coefficient

Regarding the drag coefficient which is nonlinear with respect to the angle of attack, the unsteady drag coefficient is proposed to be modeled as a function of the unsteady lift coefficient according to the parabolic drag polar model

$$C_D = C_{D_0} + K(k)\left(\bar{C}_{L_0} + C_{L_{\tilde{\alpha}}}(k)\tilde{\alpha} + C_{L_{\dot{\alpha}}}\frac{\bar{c}\dot{\alpha}}{2V_\infty}\right)^2 \tag{55}$$

where $\bar{C}_L$ is the trim lift coefficient.

Upon expansion, the unsteady drag coefficient is written as

$$C_D = \bar{C}_D + C_{D_{\tilde{\alpha}}}(k)\tilde{\alpha} + C_{D_{\dot{\alpha}}}\frac{\bar{c}\dot{\alpha}}{2V_\infty} + K(k)\left(C_{L_{\tilde{\alpha}}}(k)\tilde{\alpha} + C_{L_{\dot{\alpha}}}\frac{\bar{c}\dot{\alpha}}{2V_\infty}\right)^2 \tag{56}$$

where $\bar{C}_D$ is the trim drag coefficient.

The stability derivatives of the drag coefficient can be computed from CFD simulations by decomposing the response into a linear component and quadratic component. The unsteady drag coefficient is described by a quadratic relationship with the unsteady lift coefficient as

$$C_D = \bar{C}_D + (X_1 + iY_1)\tilde{C}_L + (X_2 + iY_2)\tilde{C}_L^2 \tag{57}$$

The quantity $\tilde{C}_L^2$ is expressed as

$$\begin{aligned}\tilde{C}_L^2 &= [(U + iW)\alpha_0 \sin k\tau]^2 = (U\alpha_0 \sin k\tau + W\alpha_0 \cos k\tau)^2 \\ &= \frac{1}{2}\left(U^2 + W^2\right)\alpha_0^2 - \frac{1}{2}\left(U^2 - W^2\right)\alpha_0^2 \cos 2k\tau + UW\alpha_0^2 \sin 2k\tau\end{aligned} \tag{58}$$

Removing the mean value from $\tilde{C}_L^2$, we write the unsteady drag coefficient as

$$\begin{aligned}\tilde{C}_D =& (X_1 + iY_1)(U + iW)\alpha_0 \sin k\tau \\ &+ (X_2 + iY_2)\left[-\frac{1}{2}\left(U^2 - W^2\right)\alpha_0^2 \cos 2k\tau + UW\alpha_0^2 \sin 2k\tau\right]\end{aligned} \tag{59}$$

The quantities X_1, X_2, Y_1, and Y_2 are evaluated as

$$X_1(k) = \frac{kU(k)\int_0^{\frac{2n\pi}{k}} \tilde{C}_D \sin k\tau d\tau + kW(k)\int_0^{\frac{2n\pi}{k}} \tilde{C}_D \cos k\tau d\tau}{n\pi\theta_0\left[U^2(k)+W^2(k)\right]} \tag{60}$$

$$Y_1(k) = \frac{-kW(k)\int_0^{\frac{2n\pi}{k}} \tilde{C}_D \sin k\tau d\tau + kU(k)\int_0^{\frac{2n\pi}{k}} \tilde{C}_D \cos k\tau d\tau}{n\pi\theta_0\left[U^2(k)+W^2(k)\right]} \tag{61}$$

$$X_2(k) = \frac{4kU(k)W(k)\int_0^{\frac{2n\pi}{k}} \tilde{C}_D \sin 2k\tau d\tau - 2k\left[U^2(k)-W^2(k)\right]\int_0^{\frac{2n\pi}{k}} \tilde{C}_D \cos 2k\tau d\tau}{n\pi\theta_0^2\left[U^2(k)+W^2(k)\right]^2} \tag{62}$$

$$Y_2(k) = \frac{k\left[U^2(k)-W^2(k)\right]\int_0^{\frac{2n\pi}{k}} \tilde{C}_D \sin 2k\tau d\tau + 2kU(k)W(k)\int_0^{\frac{2n\pi}{k}} \tilde{C}_D \cos 2k\tau d\tau}{n\pi\theta_0^2\left[U^2(k)+W^2(k)\right]^2} \tag{63}$$

To model the unsteady drag coefficient, we choose suitable proper transfer functions for the partial derivatives of $\tilde{C}_D$ with respect to $\tilde{C}_L$ and $\tilde{C}_L^2$ as

$$\frac{\partial \tilde{C}_D}{\partial \tilde{C}_L}(\bar{s}) = \frac{\sum_{i=0}^{n} f_i \bar{s}^i}{\bar{s}^n + \sum_{i=0}^{n-1} g_i \bar{s}^i} = X_1 + iY_1 \tag{64}$$

$$\frac{\partial \tilde{C}_D}{\partial \tilde{C}_L^2}(\bar{s}) = \frac{\sum_{i=0}^{n} u_i \bar{s}^i}{\bar{s}^n + \sum_{i=0}^{n-1} v_i \bar{s}^i} = X_2 + iY_2 \tag{65}$$

The transfer functions are then estimated by the frequency-domain regression in the same manner. The dynamic stability derivatives due to the unsteady drag coefficient are then estimated as

$$C_{D_{\tilde{\alpha},\dot{\alpha},q,\dot{q}}} = \frac{\partial \tilde{C}_D}{\partial \tilde{C}_L} C_{L_{\tilde{\alpha},\dot{\alpha},q,\dot{q}}} \tag{66}$$

The partial derivatives of $\tilde{C}_D$ can be expressed in the partial fraction form as

$$\frac{\partial \tilde{C}_D}{\partial \tilde{C}_L}(\bar{s}) = f_n + \sum_{i=1}^{n} \frac{t_i}{\bar{s} - q_i} \tag{67}$$

$$\frac{\partial \tilde{C}_D}{\partial \tilde{C}_L}(\bar{s}) = u_n + \sum_{i=1}^{n} \frac{v_i}{\bar{s} - w_i} \tag{68}$$

The time domain representation of the unsteady drag coefficient can then be established as

$$\tilde{C}_D = f_n \tilde{C}_L + u_n \tilde{C}_L^2 + \sum_{i=1}^{n} (\sigma_i + \eta_i) \tag{69}$$

where

$$\frac{\bar{c}\dot{\sigma}_i}{2V_\infty} = q_i \sigma_i + t_i \tilde{C}_L \tag{70}$$

$$\frac{\bar{c}\dot{\eta}_i}{2V_\infty} = w_i \eta_i + v_i \tilde{C}_L^2 \tag{71}$$

with the unsteady lift coefficient $\tilde{C}_L$ computed in the time domain as presented by Eq. (45).

III. Determination of Dynamic Stability Derivatives of Transonic Truss-Braced Wing

The dynamic stability derivative estimation method is applied to the TTBW to illustrate the procedure. A series of unsteady RANS CFD simulations of pitch and plunge oscillations of the Mach 0.8 TTBW is conducted in FUN3D.[11] The pitch center of the aircraft CG. The FUN3D tetrahedral prism mesh has about 96 million nodes. The Roe's flux-difference splitting scheme and the Spalart-Allmaras turbulence model are used in the simulations. An optimized second-order backward finite-difference scheme is used in the time integration. The pitch oscillations are about the trim points at the design lift coefficient $C_L = 0.695$ and an altitude of 46,716 ft corresponding to the mid-cruise gross weight of 130,486 lbs for the Mach 0.8 TTBW. Figure 3 is an instantaneous surface pressure contour plot of the Mach 0.8 TTBW.

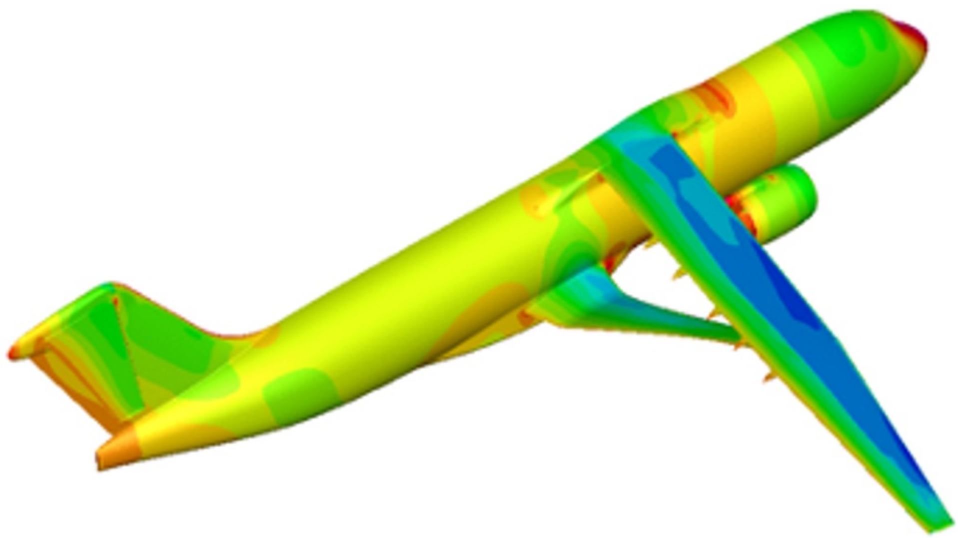

Figure 3. Mach 0.8 Transonic Truss Braced-Wing Instantaneous Pressure Contour In Pitch Oscillations

The frequency data is generated at four reduced frequencies $k = 0.01$, 0.02, 0.1, and 0.2. In addition, steady state data corresponding to $k = 0$ obtained from the steady state stability derivatives computed by steady state RANS simulations are also included. A spline fit is performed to generate the frequency response data over a reduced frequency range from 0.02 to 0.2. A regression is then performed using the second-order transfer function in Eq. (2). In some cases, A fourth-order transfer function is used to improve accuracy for the pitch rate dynamic stability derivative estimation.

A. Dynamic Stability Derivatives Due to Angle of Attack Dynamics

The dynamic stability derivatives with respect to the angle of attack are estimated first from the plunge simulation data. The plots of the unsteady lift and pitching moment, and drag coefficients versus the angle of attack due to the plunge motion for the Mach 0.8 TTBW are shown in Figs. 4(a) and (b), respectively. The analytical results using the Fourier series decomposition are compared to the FUN3D results. The agreement is excellent.

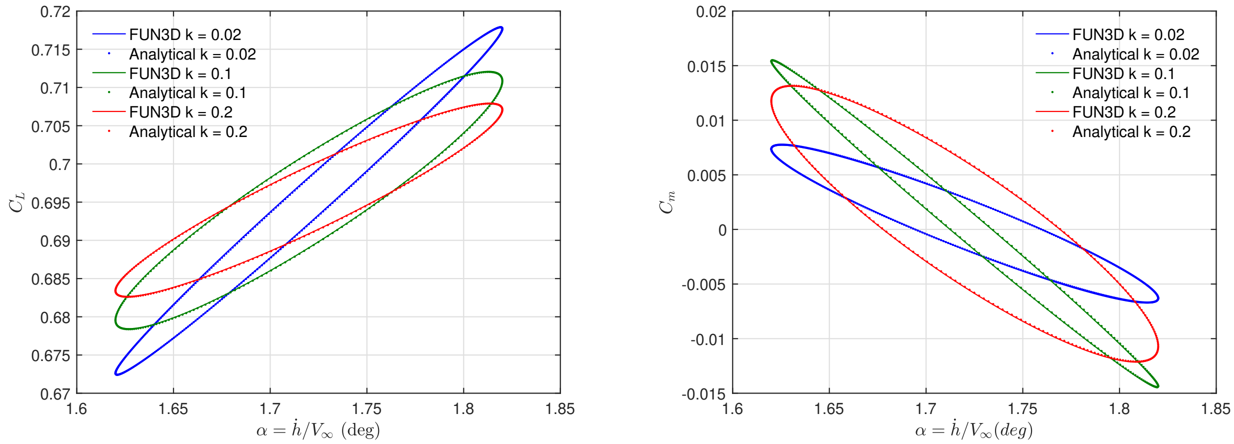

(a) (b)

Figure 4. Mach 0.8 TTBW Unsteady Lift and Pitching Moment Coefficients in Plunge

The dynamic stability derivatives with respect to the angle of attack of the Mach 0.8 obtained from the regression analysis of the plunge oscillations are obtained as

$$\frac{\partial \tilde{C}_L}{\partial \tilde{\alpha}}(\bar{s}) = \left(1 + \frac{-0.6308\bar{s}^2 - 0.0688\bar{s}}{\bar{s}^2 + 0.1995\bar{s} + 0.0099}\right) 13.1881 + 5.0637\bar{s}$$

$$C_{L_{\tilde{\alpha}}}(\bar{s}) = \left(1 + \frac{-0.6308\bar{s}^2 - 0.0688\bar{s}}{\bar{s}^2 + 0.1995\bar{s} + 0.0099}\right) 13.1881$$

$$C_{L_{\dot{\alpha}}} = 5.0637$$

$$\frac{\partial \tilde{C}_m}{\partial \tilde{\alpha}}(\bar{s}) = \left(1 + \frac{-1.8967\bar{s}^2 + 0.4803\bar{s}}{\bar{s}^2 + 0.3193\bar{s} + 0.0255}\right)(-3.5920) - 8.5490\bar{s}$$

$$C_{m_{\tilde{\alpha}}}(\bar{s}) = \left(1 + \frac{-1.8967\bar{s}^2 + 0.4803\bar{s}}{\bar{s}^2 + 0.3193\bar{s} + 0.0255}\right)(-3.5920)$$

$$C_{m_{\dot{\alpha}}} = -8.5490$$

The steady-state stability derivatives $C_{L_\alpha} = 13.1881$ and $C_{m_\alpha} = -3.5920$ are obtained at $k = 0$. The sign of the dynamic stability derivatives $C_{L_{\dot{\alpha}}}$ and $C_{m_{\dot{\alpha}}}$ are consistent with the Theordorsen's theory.

The plots of the transfer functions $\frac{\partial \tilde{C}_L}{\partial \tilde{\alpha}}(k)$ and $\frac{\partial \tilde{C}_m}{\partial \tilde{\alpha}}(k)$ obtained from the frequency-domain regression are shown in Figs. 5(a)-(b), respectively. The regression for $\frac{\partial \tilde{C}_m}{\partial \tilde{\alpha}}(k)$ is less accurate than that for $\frac{\partial \tilde{C}_L}{\partial \tilde{\alpha}}(k)$. Figures 6 (a)-(b) show the plots of the dynamic stability derivatives $C_{L_{\tilde{\alpha}}}(k)$ and $C_{m_{\tilde{\alpha}}}(k)$, respectively. Figures 7(a)-(b) show the plots of the dynamic stability derivatives $C_{L_{\dot{\alpha}}}$ and $C_{m_{\dot{\alpha}}}$ which are constant across the reduced frequency bandwidth.

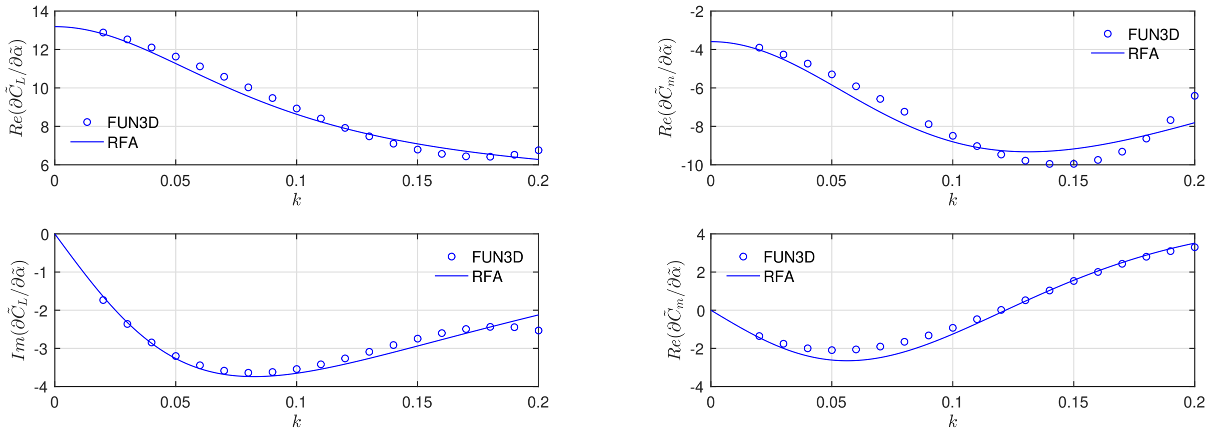

(a) (b)

Figure 5. Mach 0.8 TTBW $\dfrac{\partial \tilde{C}_L}{\partial \tilde{\alpha}}(k)$ and $\dfrac{\partial \tilde{C}_m}{\partial \tilde{\alpha}}(k)$ Regression

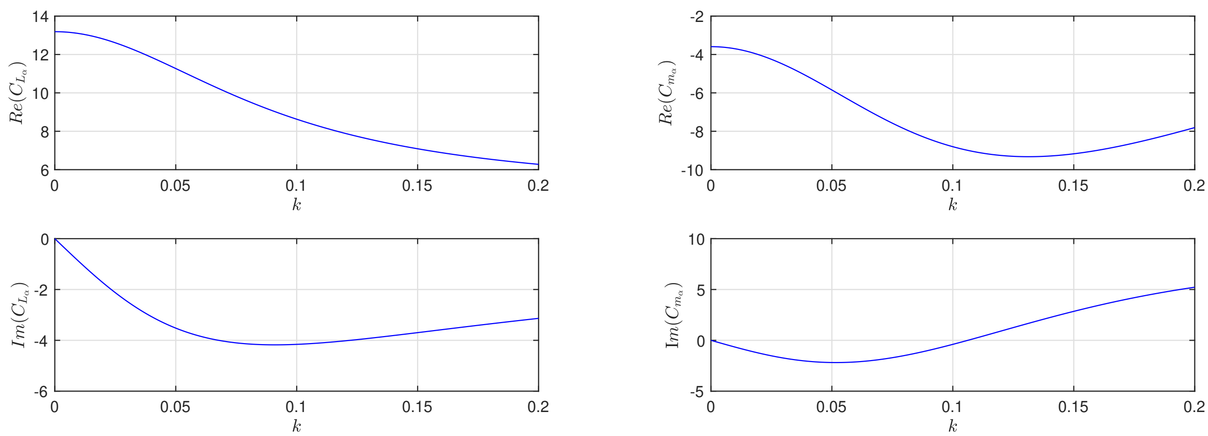

(a) (b)

Figure 6. Mach 0.8 TTBW Dynamic Stability Derivatives $C_{L_{\tilde{\alpha}}}(k)$ and $C_{m_{\tilde{\alpha}}}(k)$

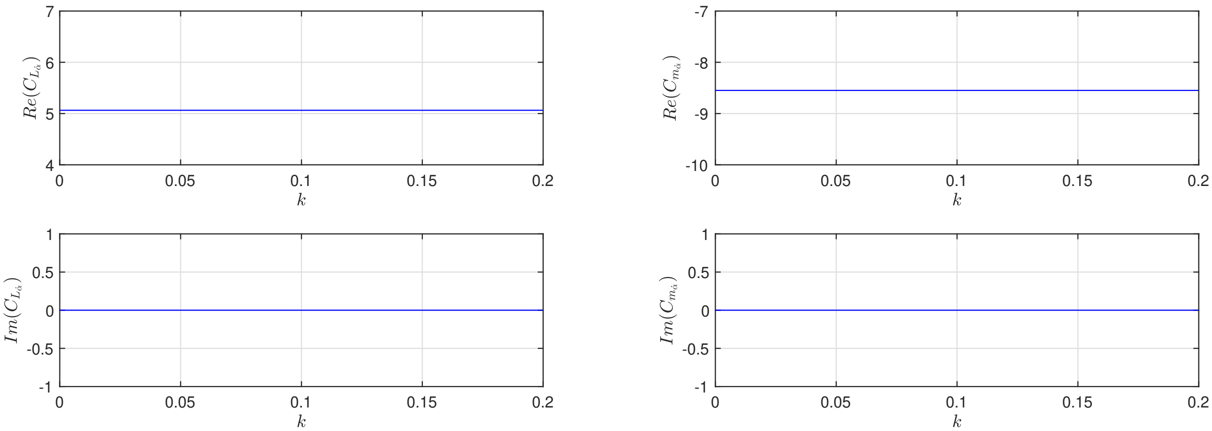

(a) (b)

Figure 7. Mach 0.8 TTBW Dynamic Stability Derivatives $C_{L_{\dot\alpha}}(k)$ and $C_{m_{\dot\alpha}}(k)$

The unsteady drag coefficient for pitch oscillations is analyzed. The unsteady drag coefficient is expressed in the component form as

$$C_D = \bar{C}_D + C_{D_{\tilde\alpha}}(k)\,\tilde\alpha + C_{D_{\tilde\alpha^2}}(k)\,\tilde\alpha^2 \tag{72}$$

The linear contribution $C_{D_{\tilde\alpha}}\tilde\alpha$ is proportional to the unsteady lift coefficient $\tilde{C}_L$, where as the quadratic contribution $C_{D_{\tilde\alpha}}\tilde\alpha$ is proportional to $\tilde{C}_L^2$. Figures 8(a)-(b) show the plots of the linear contribution $C_{D_{\tilde\alpha}}\tilde\alpha$ and quadratic contribution $C_{D_{\tilde\alpha^2}}\tilde\alpha^2$ versus the unsteady lift coefficient $\tilde{C}_L$, respectively.

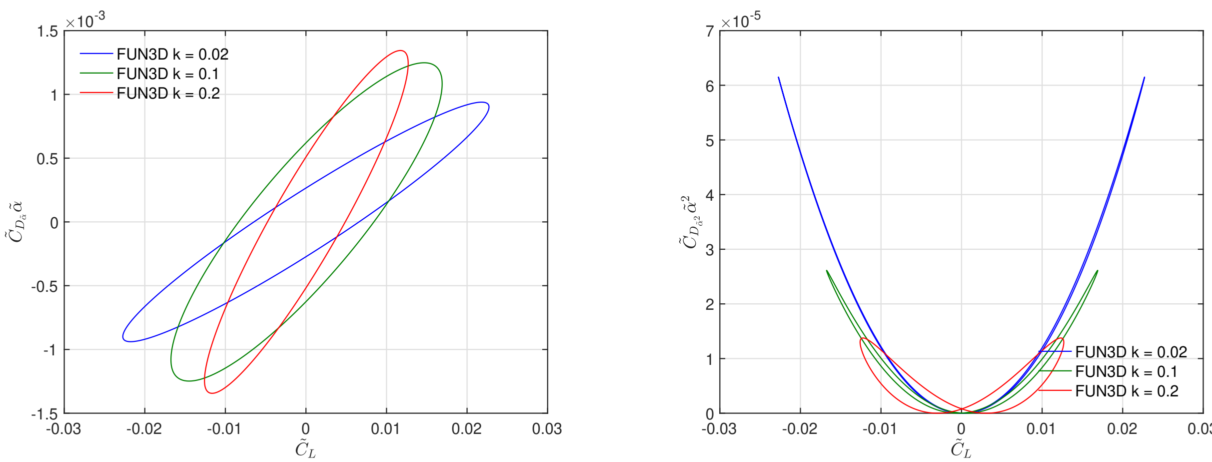

(a) (b)

Figure 8. Mach 0.8 TTBW Linear and Quadratic Unsteady Drag Coefficients $C_{D_{\tilde\alpha}}\tilde\alpha$ and $C_{D_{\tilde\alpha^2}}\tilde\alpha^2$ in Plunge

The transfer functions of the unsteady drag coefficient with respect to the unsteady lift coefficient are obtained by the frequency-domain regression as

$$\frac{\partial \tilde{C}_D}{\partial \tilde{C}_L}(\bar{s}) = \left(1 + \frac{2.03085\bar{s}^2 + 0.53971\bar{s}}{\bar{s}^2 + 0.39908\bar{s} + 0.03982}\right) 0.04004$$

$$\frac{\partial \tilde{C}_D}{\partial \tilde{C}_L^2}(\bar{s}) = \left(1 + \frac{2930.07831\bar{s}^4 - 201.54425\bar{s}^3 + 196.91406\bar{s}^2 - 8.25138\bar{s}}{\bar{s}^4 + 6.94493\bar{s}^3 + 18.06109\bar{s}^2 + 20.84655\bar{s} + 9.01090}\right) 0.11717$$

Figures 9(a)-(b) show the plots of the transfer functions of the unsteady drag coefficient.

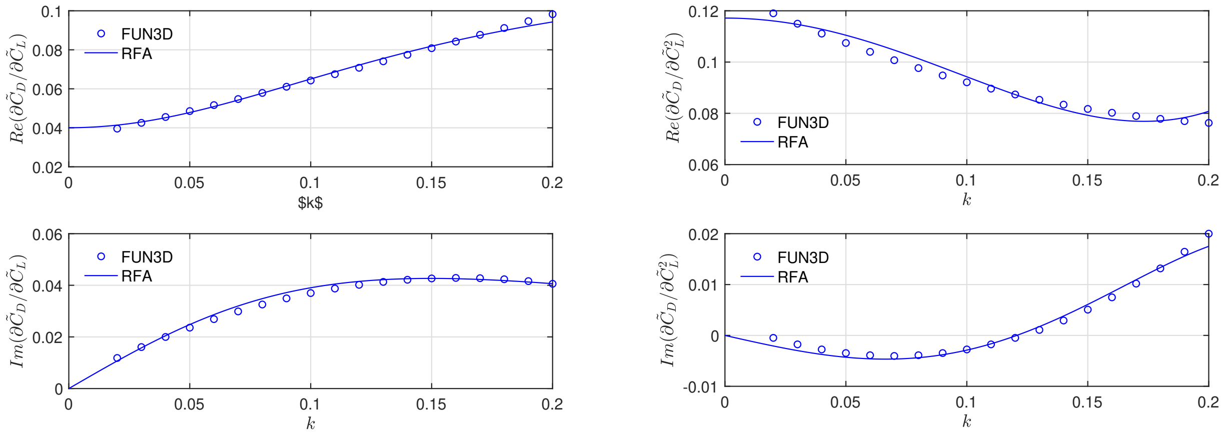

(a) (b)

Figure 9. Mach 0.8 TTBW Transfer Functions of Unsteady Drag Coefficient $\dfrac{\partial \tilde{C}_D}{\partial \tilde{C}_L}(k)$ **and** $\dfrac{\partial \tilde{C}_D}{\partial \tilde{C}_L^2}(k)$

The dynamic stability derivatives of the unsteady drag coefficient are established as

$$C_{D_{\tilde{\alpha}}}(\bar{s}) = \frac{\partial \tilde{C}_D}{\partial \tilde{C}_L}(\bar{s})\, C_{L_{\tilde{\alpha}}}(\bar{s}) = \left(1 + \frac{2.03085\bar{s}^2 + 0.53971\bar{s}}{\bar{s}^2 + 0.39908\bar{s} + 0.03982}\right)\left(1 + \frac{-0.63080\bar{s}^2 - 0.06881\bar{s}}{\bar{s}^2 + 0.19950\bar{s} + 0.00995}\right) 0.52810$$

$$C_{D_{\dot{\alpha}}}(\bar{s}) = \frac{\partial \tilde{C}_D}{\partial \tilde{C}_L}(\bar{s})\, C_{L_{\dot{\alpha}}} = \left(1 + \frac{2.03085\bar{s}^2 + 0.53971\bar{s}}{\bar{s}^2 + 0.39908\bar{s} + 0.03982}\right) 0.20277$$

The steady-state stability derivative $C_{D_\alpha} = 0.52810$ is obtained at $k = 0$. The L/D can be estimated by the ratio of the steady-state stability derivative C_{L_α} to the steady-state stability derivative C_{D_α}. The L/D is estimated to be 24.97. This value is similar to the maximum $L/D = 21.16$ at the design $C_L = 0.695$ computed by steady-state RANS solution in FUN3D. The small difference could be due to the uncertainty in the analysis.

The steady-state stability derivatives with respect to the angle of attack are compared to those obtained by steady-state simulations in both FUN3D and VSPAERO. The VSPAERO model includes a transonic small disturbance correction and an integral boundary layer model.[12] Table 1 shows the comparison of the steady-state derivatives C_{L_α}, C_{m_α}, and C_{D_α} for the three different sets of results. The agreement among them is excellent.

	Unsteady FUN3D	Steady-State FUN3D	VSPAERO
C_{L_α}	13.1881	13.3577	13.2762
C_{m_α}	-3.5920	-3.6312	-3.6751
C_{D_q}	0.5281	0.5273	0.5209

Table 1. Comparison of Steady-State Stability Derivatives with Respect to Angle of Attack

B. Dynamic Stability Derivatives Due to Pitch Rate Dynamics

In order to estimate the dynamic stability derivatives with respect to the pitch rate, the differential unsteady lift and pitching moment coefficients are computed first via Eq. (48) or (52). Figures 10(a)-(b) are the plots of the unsteady lift and pitching moment coefficients versus the pitch angle for the Mach 0.8 TTBW, respectively. The analytical results using the Fourier series decomposition are compared to the FUN3D results. The agreement is excellent. The plots of the differential unsteady lift and pitching moment coefficients versus the nondimensional pitch rate are shown in Figs. 11(a) and (b), respectively. The effect of aerodynamic lag due to the pitch rate dynamics is more pronounced for the unsteady lift coefficient than for the unsteady pitching moment coefficient, as indicated by the widths of the elliptical hystereses.

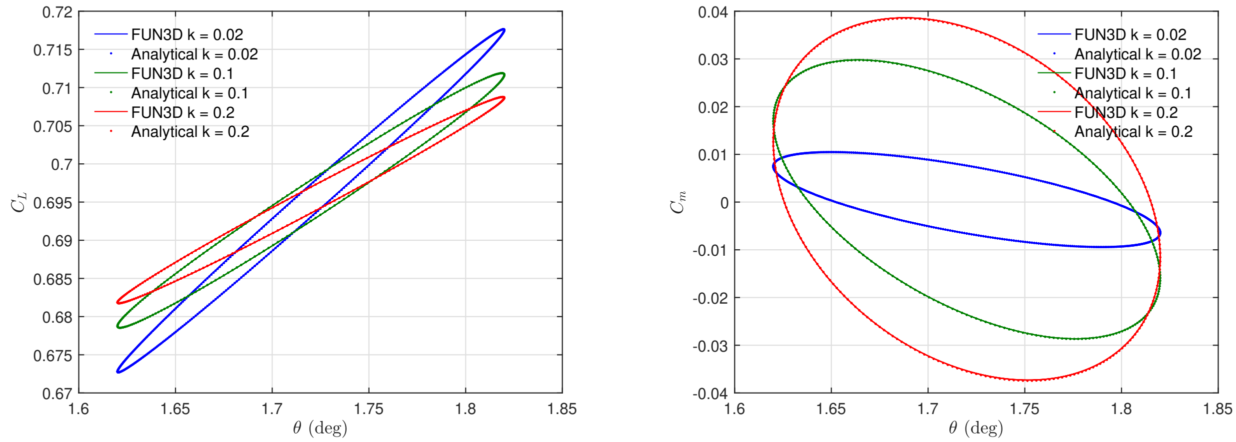

(a) (b)

Figure 10. Mach 0.8 TTBW Unsteady Lift and Pitching Moment Coefficients in Pitch

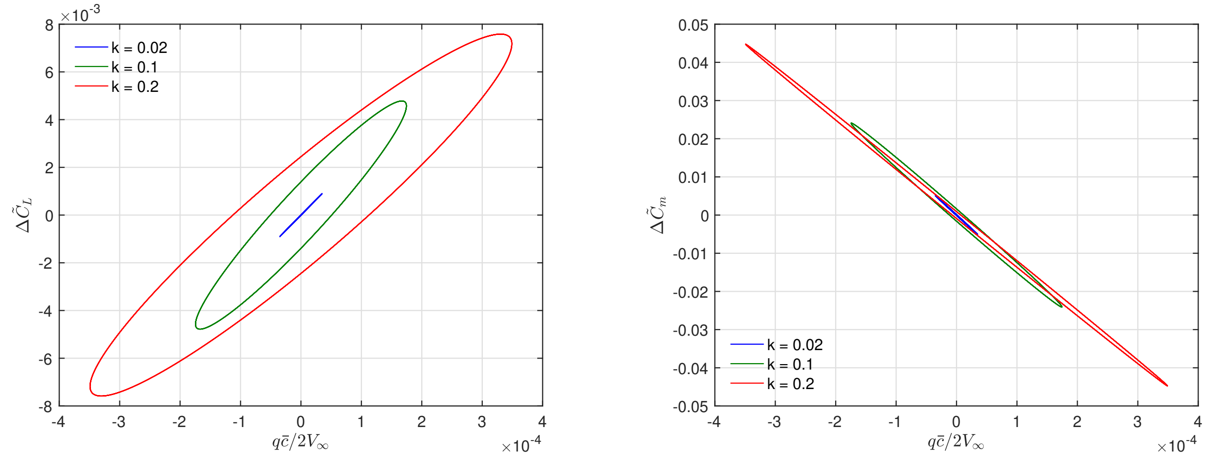

(a) (b)

Figure 11. Mach 0.8 TTBW Differential Unsteady Lift and Pitching Moment Coefficients in Pitch

The dynamic stability derivatives with respect to the pitch rate of the Mach 0.8 obtained from the regression analysis of the pitch oscillations are obtained as

$$\frac{\partial \Delta\tilde{C}_L}{\partial \tilde{q}}(\bar{s}) = \left(1 + \frac{14.8692\bar{s}^4 + 16.1254\bar{s}^3 + 3.6476\bar{s}^2 + 0.3994\bar{s}}{\bar{s}^4 + 1.5466\bar{s}^3 + 0.8966\bar{s}^2 + 0.2309\bar{s} + 0.0223}\right) 25.0453 - 496.4001\bar{s}$$

$$C_{L_{\tilde{q}}}(\bar{s}) = \left(1 + \frac{14.8692\bar{s}^4 + 16.1254\bar{s}^3 + 3.6476\bar{s}^2 + 0.3994\bar{s}}{\bar{s}^4 + 1.5466\bar{s}^3 + 0.8966\bar{s}^2 + 0.2309\bar{s} + 0.0223}\right) 25.0453$$

$$C_{L_{\dot{\tilde{q}}}} = -496.4001$$

$$\frac{\partial \Delta\tilde{C}_m}{\partial \tilde{q}}(\bar{s}) = \left(1 + \frac{5.7138675\bar{s}^4 + 2.2546\bar{s}^3 + 0.4550\bar{s}^2 + 0.0272\bar{s}}{\bar{s}^4 + 1.1741\bar{s}^3 + 0.5169\bar{s}^2 + 0.1011\bar{s} + 0.0074}\right)(-146.0690) + 714.7804\bar{s}$$

$$C_{m_{\tilde{q}}}(\bar{s}) = \left(1 + \frac{5.7138675\bar{s}^4 + 2.2546\bar{s}^3 + 0.4550\bar{s}^2 + 0.0272\bar{s}}{\bar{s}^4 + 1.1741\bar{s}^3 + 0.5169\bar{s}^2 + 0.1011\bar{s} + 0.0074}\right)(-146.0690)$$

$$C_{m_{\dot{q}}} = 714.7804$$

We obtain the steady-state stability derivatives $C_{L_q} = 25.0453$ and $C_{m_q} = -146.0690$ at $k = 0$. The plots of the transfer functions $\frac{\partial \Delta \tilde{C}_L}{\partial \tilde{q}}(k)$ and $\frac{\partial \Delta \tilde{C}_m}{\partial \tilde{q}}(k)$ obtained from the frequency-domain regression are shown in Figs. 12(a)-(b), respectively. Figures 13(a)-(b) show the plots of the dynamic stability derivatives $C_{L_{\tilde{q}}}(k)$ and $C_{m_{\tilde{q}}}(k)$. Figures 14(a)-(b) show the plots of the dynamic stability derivatives $C_{L_{\dot{q}}}$ and $C_{m_{\dot{q}}}$ which are constant across the reduced frequency bandwidth.

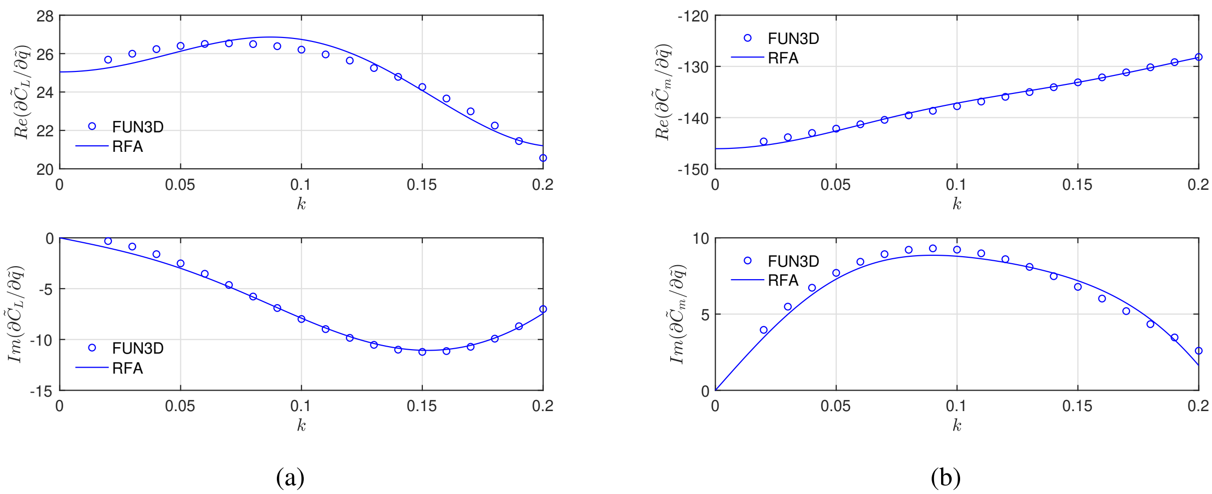

Figure 12. Mach 0.8 TTBW $\frac{\partial \Delta \tilde{C}_L}{\partial \tilde{q}}(k)$ and $\frac{\partial \Delta \tilde{C}_m}{\partial \tilde{q}}(k)$ Regression

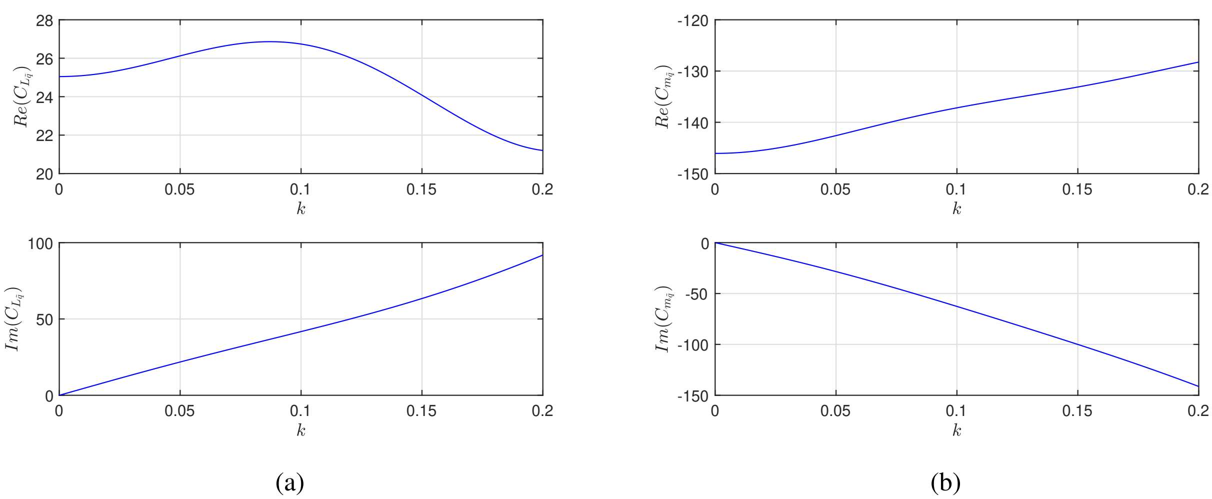

Figure 13. Mach 0.8 TTBW Dynamic Stability Derivatives $C_{L_{\tilde{q}}}(k)$ and $C_{m_{\tilde{q}}}(k)$

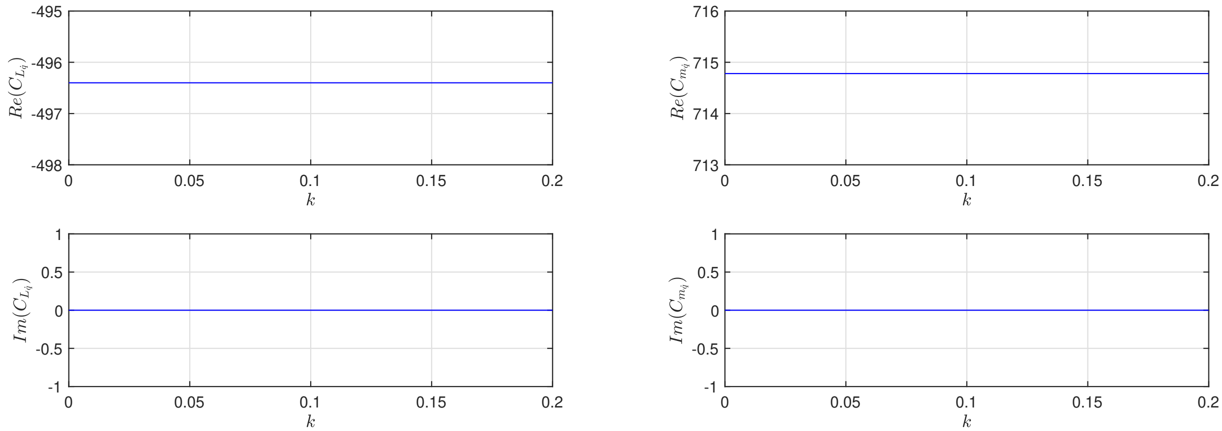

(a) (b)

Figure 14. Mach 0.8 TTBW Dynamic Stability Derivatives $C_{L_{\dot{q}}}(k)$ and $C_{m_{\dot{q}}}(k)$

The unsteady drag coefficient for the pitch oscillations is also analyzed. The plots of the linear contribution $C_{D_{\tilde{\alpha}}}\tilde{\alpha}$ and quadratic contribution $C_{D_{\tilde{\alpha}^2}}\tilde{\alpha}^2$ versus the unsteady lift coefficient $\tilde{C}_L$ are shown in Fig. 15(a)-(b), respectively.

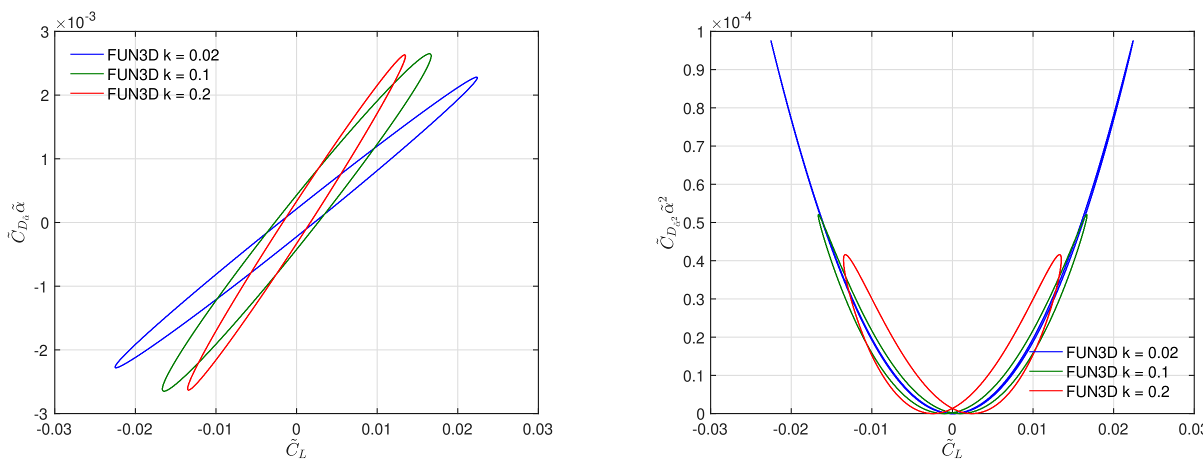

(a) (b)

Figure 15. Mach 0.8 TTBW Linear and Quadratic Unsteady Drag Coefficients $C_{D_{\tilde{\alpha}}}\tilde{\alpha}$ and $C_{D_{\tilde{\alpha}^2}}\tilde{\alpha}^2$ in Pitch

The transfer functions of the unsteady drag coefficient with respect to the unsteady lift coefficient are obtained by the frequency-domain regression as

$$\frac{\partial \tilde{C}_D}{\partial \tilde{C}_L}(\bar{s}) = \left(1 + \frac{-1.1500\bar{s}^2 + 0.5576\bar{s}}{\bar{s}^2 + 0.5630\bar{s} + 0.0668}\right) 0.0907$$

$$\frac{\partial \tilde{C}_D}{\partial \tilde{C}_L^2}(\bar{s}) = \left(1 + \frac{862.7758\bar{s}^4 + 10.5057\bar{s}^3 + 8.7099\bar{s}^2 - 2.5961\bar{s}}{\bar{s}^4 + 5.7730\bar{s}^3 + 12.4761\bar{s}^2 + 11.9616\bar{s} + 4.2926}\right) 0.1910$$

Figures 16 (a)-(b) show the plots of the transfer functions of the unsteady drag coefficient. The transfer function $\frac{\partial \tilde{C}_D}{\partial \tilde{C}_L^2}(k)$ is more difficult to obtained and therefore is less accurate than the transfer function $\frac{\partial \tilde{C}_D}{\partial \tilde{C}_L}(k)$. A 4$^{\text{th}}$-order regression is needed to increase accuracy which still could be further improved with perhaps higher-order regression.

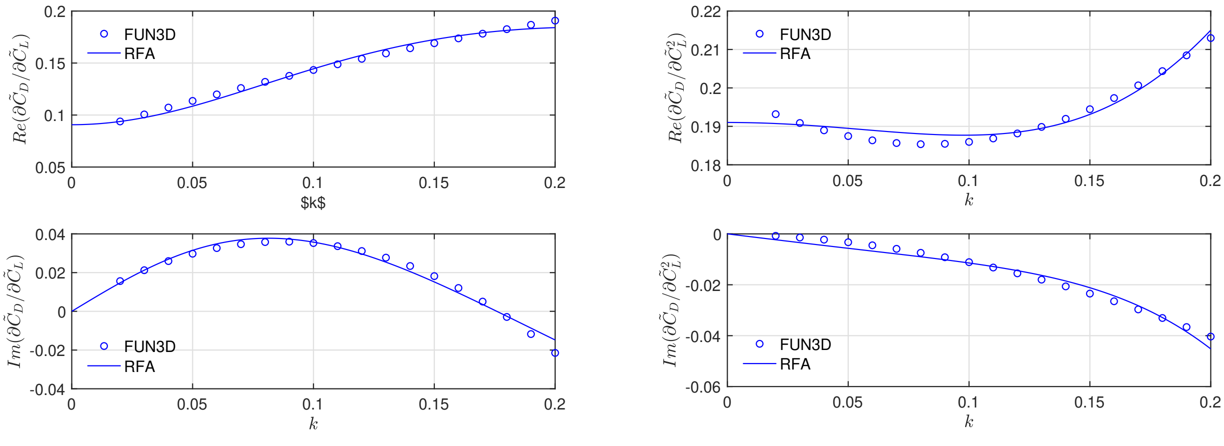

(a) (b)

Figure 16. Mach 0.8 TTBW Transfer Functions of Unsteady Drag Coefficient $\frac{\partial \tilde{C}_D}{\partial \tilde{C}_L}(k)$ and $\frac{\partial \tilde{C}_D}{\partial \tilde{C}_L^2}(k)$

The dynamic stability derivatives of the unsteady drag coefficient are then established as

$$
\begin{aligned}
C_{D_{\tilde{q}}}(\bar{s}) &= \frac{\partial \tilde{C}_D}{\partial \tilde{C}_L}(\bar{s})\, C_{L_{\tilde{q}}}(\bar{s}) \\
&= \left(1+\frac{-1.1500\bar{s}^2+0.5576\bar{s}}{\bar{s}^2+0.5630\bar{s}+0.0668}\right)\left(1+\frac{14.8692\bar{s}^4+16.1254\bar{s}^3+3.6476\bar{s}^2+0.3994\bar{s}}{\bar{s}^4+1.5466\bar{s}^3+0.8966\bar{s}^2+0.2309\bar{s}+0.0223}\right)2.2714
\end{aligned}
$$

$$
C_{D_{\dot{q}}}(\bar{s}) = \frac{\partial \tilde{C}_D}{\partial \tilde{C}_L}(\bar{s})\, C_{L_{\dot{q}}} = \left(1+\frac{-1.1500\bar{s}^2+0.5576\bar{s}}{\bar{s}^2+0.5630\bar{s}+0.0668}\right)3.01233
$$

The steady-state stability derivatives of the drag coefficient $C_{D_q} = 2.2714$ is obtained at $k = 0$.

The steady-state stability derivatives with respect to the pitch rate are compared to those obtained by steady-state simulations in VSPAERO. Table 2 shows the comparison of the steady-state derivatives C_{L_q}, C_{m_q}, and C_{D_q} which are in excellent agreement, except for the steady-state derivative C_{D_q} which is in reasonable agreement.

	FUN3D	VSPAERO
C_{L_q}	25.0453	24.7797
C_{m_q}	-146.0690	-143.4436
C_{D_q}	2.2714	1.8328

Table 2. Comparison of Steady-State Stability Derivatives with Respect to Pitch Rate

IV. Conclusion

This paper presents a new method which has been developed to extract dynamic stability derivatives from unsteady RANS CFD simulations of a full aircraft configuration in high-speed transonic flight. The aircraft is the Mach 0.8 Transonic Truss-Braced Wing developed by Boeing under a NASA contract. A series of pitch and plunge oscillations are simulated in FUN3D over a range of the reduced frequency. A frequency-domain regression is then formulated to capture the frequency dependency of the dynamic stability derivatives obtained from the unsteady RANS simulation data for the pitch and plunge oscillations. The contribution of the angle of attack dynamics to the stability is determined by the regression of the unsteady aerodynamic coefficients for the plunge motion. On the other hand, the contribution of the pitch rate dynamics to the stability is determined by the regression of the differential unsteady aerodynamic coefficients for the pitch motion upon the removal of the angle of attack contribution by the plunge motion. From the computed dynamic stability derivatives, the steady-state stability derivatives are extracted as the zero reduced frequency values. These steady-state stability derivatives are compared to the steady-state stability derivatives obtained from the steady-state simulations performed in FUN3D and VSPAERO. Excellent agreement among the results is obtained.

Acknowledgment

The authors wish to acknowledge NASA Advanced Air Transport Technology project for the funding support of this work. The authors also acknowledge Boeing Research and Technology and in particular Christopher Droney, Neal Harrison, Michael Beyar, Eric Dickey, and Anthony Sclafani, along with the NASA technical POC, Gregory Gatlin, for their research conducted under the NASA BAART contracts NNL10AA05B and NNL16AA04B. The research published in this paper is made possible by the technical data and wind tunnel test data furnished under these BAART contracts.

References

[1] Wang, F., and Chen, L., "Numerical Prediction of Stability Derivatives for Complex Configurations," Procedia Engineering 99 (2015) 1561-1575.

[2] Ghoreyshi M., Bergeron K., Lofthouse, A., and Cummings R., "CFD Calculation of Stability and Control Derivatives For Ram-Air Parachutes," AIAA Applied Aerodynamics Conference, AIAA-2016-1536, 2016.

[3] Murmann, S., "A Reduced-Frequency Approach for Calculating Dynamic Derivatives," AIAA Aerospace Sciences Meeting, AIAA-2005-0840, 2005.

[4] Theodorsen, T., "General Theory of Aerodynamic Instability and the mechanism of Flutter", NACA Report No. 496, 1949.

[5] Bradley, M. K. and Droney, C. K., "Subsonic Ultra Green Aircraft Research: Phase I Final Report," NASA Contractor Report NASA/CR-2011-216847, Boeing Research and Technology, April 2011.

[6] Bradley, M. K., Droney, C. K., and Allen, T. J., "Subsonic Ultra Green Aircraft Research Phase II: N+4 Advanced Concept Development," NASA Contractor Report NASA/CR-2012-217556, Boeing Research and Technology, May 2012.

[7] Nguyen, N., Fugate, J., Kaul, U., and Xiong, J., "Flutter Analysis of the Transonic Truss-Braced Wing Aircraft Using Transonic Correction," AIAA Structural Dynamics Conference, AIAA-2019-0217, January 2019.

[8] Kaul, U. and Nguyen, N., "RANS Simulations of a Pitching and Plunging VCCTEF Airfoil Toward a Transonic Flutter Model," AIAA Structural Dynamics Conference, AIAA-2019-2037, January 2019.

[9] Kaul, U. and Nguyen, N., "Extending A Correction Method for Unsteady Transonic Aerodynamics as Applied to Variable Camber Continuous Trailing Edge Flap," AIAA Applied Aerodynamic Conference, AIAA-2019-3157, June 2019.

[10] Nguyen, N. and Xiong, J., "Transonic Correction to Theodorsen's Theory for Oscillating Airfoil in Pitch and Plunge Toward Flutter," AIAA Structural Dynamics Conference, AIAA-2021-1913, January 2021.

[11] Xiong, J. and Nguyen, N., "Steady and Unsteady Simulations of Transonic Truss-Braced Wing Aircraft for Flight Dynamic Stability Analysis," AIAA Applied Aerodynamics Conference, June 2022.

[12] Chaparro, D., Fujiwara, G. E., Ting, E., and Nguyen, N. T., "Transonic and Viscous Potential Flow Method Applied to Flexible Wing Transport Aircraft," 35th AIAA Applied Aerodynamics Conference, AIAA-2017-4221, June 2017.